

Fast Range Point Migration Method for Weapon Detection using Ultra-Wideband Radar

Takuya Sakamoto*,

IRCTR, Delft University of Technology

Mekelweg 4, 2628 CD Delft, the Netherlands

Graduate School of Informatics, Kyoto University

Yoshida-Honmachi, Sakyo-ku, 606-8501 Kyoto, Japan

Timofey Savelyev, Pascal Aubry, and Alexander Yarovoy

IRCTR, Delft University of Technology

Mekelweg 4, 2628 CD Delft, the Netherlands

Abstract—Radar-based security systems are of considerable importance because of their potential for detecting concealed weapons, particularly when they are in jackets or bags. To achieve this capability, the system has to achieve high-resolution and high-speed processing simultaneously. Many of the conventional technologies have focused on resolution, not speed. Recently, high-speed imaging methods for ultra-wideband (UWB) radars have been developed, amongst which the fast range-point-migration (RPM) method is the most promising technique because of its robustness against interference and noise. We apply the fast RPM method to measurement data with a mannequin and a gun to investigate the method's capability for detecting a weapon.

I. INTRODUCTION

Ultra-wide-band (UWB) radar imaging is a promising technology for detecting concealed weapons in public areas. A variety of imaging methods for UWB radars have been developed [1], [2], [3], [4], [5], [6], [7]. Although one of the important features required by these security systems is fast calculation speed, many of the existing imaging methods do not satisfy this condition. To meet this need, SEABED (shape estimation algorithm based on the boundary scattering transform (BST) and extraction of directly scattered waves) has been proposed [8], [9], [10], [11], [12], using a reversible bistatic-IBST (inverse boundary scattering transform). SEABED calculates the inclination of the peak point sequence that is required by the bistatic-IBST. SEABED has been demonstrated to generate accurate images only for simply-shaped targets. This is because complex-shaped targets generate overlapping echoes that interfere with one another, making it difficult to estimate the inclination of echo sequences.

The range-point-migration (RPM) method was developed to resolve this difficulty [13], [14] and can obtain images even for complex-shaped targets. This method calculates the inclination of peak sequences using an optimization technique to avoid the interference problem. Although the RPM method produces better-quality images than SEABED, it is not as fast because the optimization processing is time-consuming. We have developed a new fast-RPM method that replaces the optimization process with weighted averaging to improve the processing speed. In this study, we investigate the capability of the fast-RPM method to detect a gun placed on a mannequin to demonstrate its performance as a security system for detecting concealed weapons.

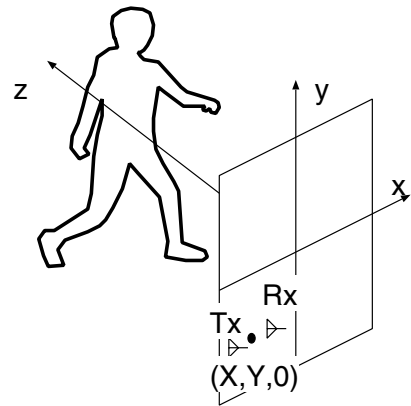


Fig. 1. System model with a pair of antennas scanning in the ($z = 0$) plane.

II. SYSTEM MODEL

We use a three-dimensional UWB radar imaging system in our investigation. Fig. 1 shows the system model assumed in this study. The measurement system consists of a transmitter-receiver pair positioned in the $z = 0$ plane along the x axis at a fixed distance $2d$. The midpoint between the transmitter and receiver is labeled $(X, Y, 0)$. With the transmitter-receiver pair being rastered at discrete intervals across a portion of the $z = 0$ plane, UWB pulses are transmitted and pulse echoes are received. The received signals contain not only echoes from the target but also a coupling signal that propagates directly from the transmitter to the receiver. To eliminate this coupling signal, the background signal, measured without a target prior to the actual measurement, is subtracted from the received signal. Given the antennae midpoint $(X, Y, 0)$, the signal received is labeled $s(X, Y, Z)$ and $Z = ct/2$, where c is the speed of the electromagnetic wave and t is the time interval between transmission and reception.

III. 3-D BISTATIC IBST

This section describes the procedures using in the 3-D bistatic IBST [12]. First, we extract peaks, which satisfy

$$\frac{\partial}{\partial Z} s(X, Y, Z) = 0, \quad (1)$$

$$|s(X, Y, Z)| > T_s, \quad (2)$$

where T_s is a constant threshold introduced to prevent the pick-up of noise. These peaks are indexed as (X_i, Y_i, Z_i) for $(i = 1, 2, \dots, N)$. The corresponding amplitudes of these peaks are, for simplicity, denoted $s_i = s(X_i, Y_i, Z_i)$. For a single simple-shaped target, these points are easily connected sequentially to form multiple curved surfaces $Z(X, Y)$. This function is called a quasi-wavefront.

Next, we apply the following bistatic-IBST to the quasi-wavefronts to obtain images:

$$x = X - \frac{2Z^3 Z_X}{Z^2 - d^2 + \sqrt{(Z^2 - d^2)^2 + 4d^2 Z^2 Z_X^2}}, \quad (3)$$

$$y = Y + Z_Y \{d^2(x - X)^2 - Z^4\} / Z^3, \quad (4)$$

$$z = \sqrt{Z^2 - d^2 - (y - Y)^2 - \frac{(Z^2 - d^2)(x - X)^2}{Z^2}}, \quad (5)$$

using for simplicity $Z_X = \partial Z / \partial X$ and $Z_Y = \partial Z / \partial Y$.

The variables we need to successfully apply the bistatic-IBST are X, Y, Z, Z_X and Z_Y , of which X, Y and Z are known. To obtain derivatives Z_X and Z_Y , the peaks must be connected when forming the curved surfaces. Since this is not an easy task for complex-shaped targets, we refrain from using the bistatic-IBST.

IV. FAST RPM METHOD

In this section, we explain the fast-RPM method. We replace the optimization process of the RPM method with the following weighted average approach. The relative orientation of the peaks around the i -th peak is estimated with a weighted average as:

$$\theta_i = \frac{\sum_{j \neq i, Y_j = Y_i} w_{i,j} \tan^{-1} \left(\frac{Z_i - Z_j}{X_i - X_j} \right)}{\sum_{j \neq i, Y_j = Y_i} w_{i,j}}, \quad (6)$$

where

$$w_{i,j} = |s_i s_j| \exp \left(-\frac{(X_i - X_j)^2}{\sigma_X^2} - \frac{(Z_i - Z_j)^2}{\sigma_Z^2} \right) \quad (7)$$

and $\left| \tan^{-1} \left(\frac{Z_i - Z_j}{X_i - X_j} \right) \right| < \pi/4$, and the summations are over pairs of peaks with the same sign in the 2nd derivative i. e.

$$s_{zz}(X_i, Y_i, Z_i) s_{zz}(X_j, Y_j, Z_j) > 0, \quad (8)$$

where $s_{zz}(X, Y, Z) = \frac{\partial^2}{\partial Z^2} s(X, Y, Z)$. Figure 2 shows the schematic of the procedure in the fast RPM method. As in this figure, the inclination of points around the i -th point is calculated by averaging the angle between the i -th and j -th points over all j close to the i -th point. By finding the θ_i using Eq. (6), we obtain an estimate of the quasi-wavefront orientation. Next, we calculate $Z_X = \tan(\theta_i)$. In the same way, we can estimate Z_Y . Finally, these derivatives are substituted into Eqs. (3), (4), and (5), to obtain target images.

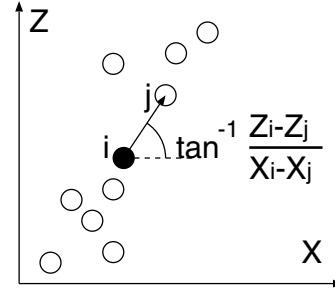


Fig. 2. Schematic of fast RPM method.

V. IMAGING PROCEDURES USING DIFFRACTION STACK MIGRATION AND FAST RPM METHOD

Diffraction-stack migration calculated a target image as

$$I_{DS}(x, y, z) = \sum_{X, Y} s(X, Y, \sqrt{(x - X)^2 + (y - Y)^2 + z^2}) \quad (9)$$

for $-50\text{cm} \leq x \leq 50\text{cm}$, $-80\text{cm} \leq y \leq 80\text{cm}$ and $47\text{cm} \leq z \leq 67\text{cm}$ with a 1 cm grid width along x and y axes, and a 0.5 cm grid width along z axis.

The fast RPM methods extracts 15 peaks for each antenna position. We set $\sigma_X = \sigma_Y = 0.8\text{cm}$, $\sigma_Z = 0.3\text{cm}$ and $\sigma_\theta = \pi/100$. The i -th target image point (x_i, y_i, z_i) obtained from Eqs. (3), (4) and (5) is weighted with amplitude $|s_i|$ to generate a volume image $I_{FRPM}(x, y, z)$.

Although both methods generate three-dimensional images, we show two-dimensional images in this paper to quantitatively display the results. The volume image $I_{DS}(x, y, z)$ or $I_{FRPM}(x, y, z)$ is projected onto the x - y plane by:

$$z(x, y) = \arg \max_z |I(x, y, z)|. \quad (10)$$

Finally, we apply a median filter to eliminate noise from the images generated by the both methods. A 3×3 -pixel box window is employed. A median value is calculated for each box and replace the central pixel with the median value.

VI. PERFORMANCE EVALUATION

We apply the fast-RPM method and diffraction stack migration to experimental data to investigate their performance in detecting weapons attached to a mannequin. In our measurements, a human body phantom with a conductive surface was placed 53 cm from the antenna scanning plane. Figure 3 shows a metallic mannequin with a gun used as a target for our measurements. The gun is suspended by a fine thread that does not affect the measurement.

The data are acquired in the frequency domain, and Fourier-transformed to obtain the time-domain data. We employed an Agilent PNA E8364B to sweep frequency from 5.0 GHz to 25.0 GHz with 2001 points. From these data points, we extracted 350 points from 2.5 nsec to 6.0 nsec in the time domain for signal processing. The central frequency of the received signals is 13.4 GHz and its 10-dB bandwidth is 14.9 GHz. The transmitted power is 2.0 dBm. The distance



Fig. 3. Experimental setup with a mannequin and a weapon.

between the transmitting and receiving antennas is 5.0 cm, giving $d = 2.5$ cm. The antennas scanned from locations at 1.0 cm intervals ranging from $-37.0\text{cm} \leq X \leq 37.0\text{cm}$ and $-75.0\text{cm} \leq Y \leq 75.0\text{cm}$. The total number of measuring points is $75 \times 151 = 11,325$.

Figures 4 and 5 show the images produced by the diffraction stack migration and fast RPM methods for a mannequin without a gun. These images display a human body, and we see no anomaly that suggests the existence of a weapon. The calculation times are 483.85 s and 2.81 s for the diffraction stack migration and the fast RPM method on a computer with Intel Core i7 processor with 8 GB memory. The fast RPM method is 172.2 times faster than diffraction stack migration in this case. Note that the abovementioned processing time does not include time for scanning antennas. In general, it takes longer to scan antennas, which should be properly addressed to achieve real-time imaging.

Figures 6 and 7 show the images obtained with the diffraction stack migration and fast RPM methods for a mannequin with a gun. In the both images we see an image of a gun at approximately $(-10.0\text{cm}, 30.0\text{cm})$. The image generated by the fast RPM method is more detailed than that generated by the diffraction stack migration method. The calculation time for the fast RPM method is again 170.0 times faster than for the diffraction stack migration method.

The measurements have been conducted under the assumption that the target is standing still without moving. The images generated by the imaging methods for a target in motion would be blurred, which is an important future task.

VII. CONCLUSIONS

In this study, we investigated the weapon-detection capability of the conventional diffraction stack migration and the fast RPM methods to compare them in terms of the image quality and calculation speed. Measurements are conducted using a UWB radar system with a mechanical scanner and a metallic mannequin with and without a weapon. The imaging capability of the fast RPM method is better at depicting the

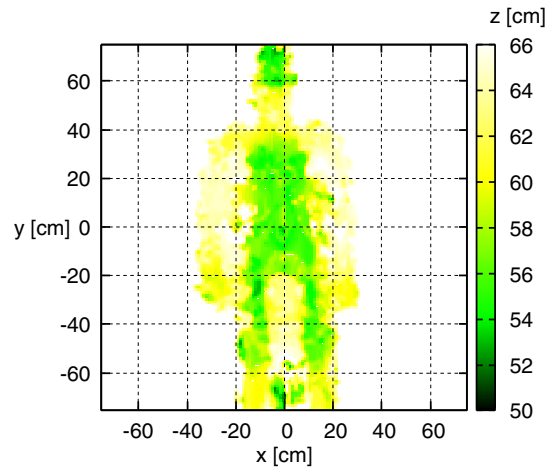


Fig. 4. Image generated using the diffraction stack migration method from the measured data with a mannequin without a gun (calculation time: 483.85 s).

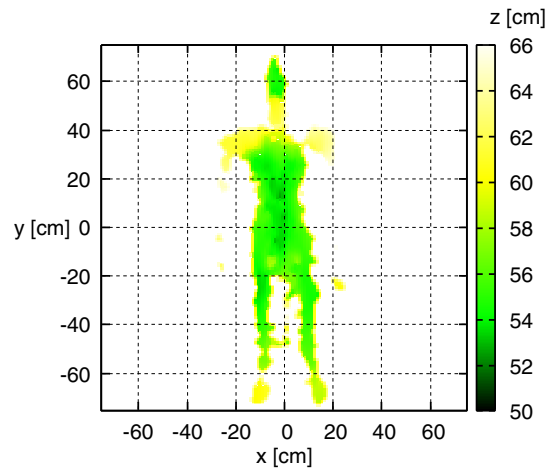


Fig. 5. Image generated using the fast RPM method from the measured data with a mannequin without a gun (calculation time: 2.81 s).

detailed shape of a weapon than the diffraction stack migration method. The signal processing speed of the fast RPM method is 170 times greater than that for the diffraction stack migration method. These results indicate the fast RPM method is an attractive candidate for a next-generation security system that can detect weapons carried on a human body.

REFERENCES

- [1] A. G. Yarovoy, T. G. Savelyev, P. J. Aubry, P. E. Lys, L. P. Ligthart, "UWB array-based sensor for near-field imaging," *IEEE Transactions on Microwave Theory and Techniques*, vol. 55, no. 6, part 2, pp. 1288-1295, June 2007.
- [2] X. Zhuge, A. G. Yarovoy, T. Savelyev, L. Ligthart, "Modified Kirchhoff migration for UWB MIMO array-based radar imaging" *IEEE Transactions on Geoscience and Remote Sensing*, vol. 48, no. 6, pp. 2692-2703, 2010.
- [3] X. Zhuge, and A. Yarovoy, "A sparse aperture MIMO-SAR based UWB imaging system for concealed weapon detection," *IEEE Transactions on Geoscience and Remote Sensing*, vol. 49 no. 1, pp. 509-518, 2011.

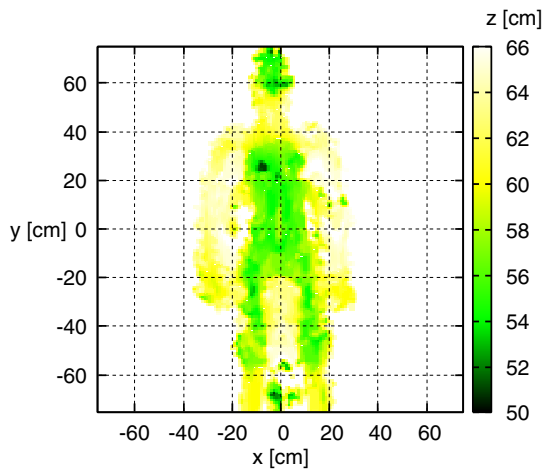


Fig. 6. Image generated using the diffraction stack migration method from the measured data with a mannequin with a gun (calculation time: 484.50 sec).

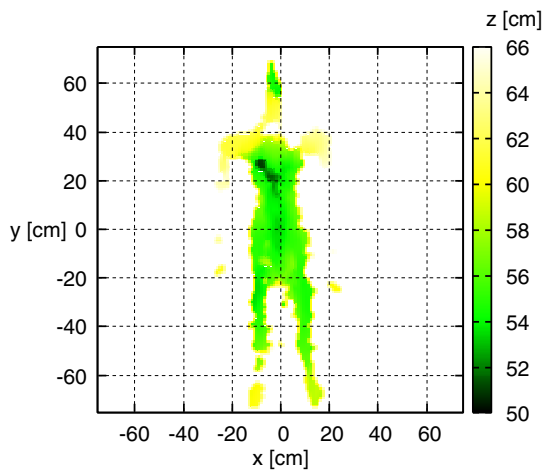


Fig. 7. Image generated using the fast RPM method from the measured data with a mannequin with a gun (calculation time: 2.85 s).

vol. 15, pp. 269–272, 2008.

[11] R. Salman, I. Willms, "In-Wall Object Recognition based on SAR-like Imaging by UWB-Radar," Proc. 8th European Conference on Synthetic Aperture Radar (EUSAR), 2010.

[12] S. Kidera, Y. Kani, T. Sakamoto and T. Sato, "A fast and high-resolution 3-D imaging algorithm with linear array antennas for UWB pulse radars," IEICE Trans. on Communications, vol. E91-B, no. 8, pp. 2683–2691, 2008.

[13] S. Kidera, T. Sakamoto and T. Sato, "Accurate UWB Radar 3-D Imaging Algorithm for Complex Boundary without Range Points Connections," IEEE Trans. Geoscience and Remote Sensing, vol. 48, no. 4, pp. 1993–2004, 2010.

[14] R. Salman and I. Willms, "3D UWB Radar super-resolution imaging for complex objects with discontinuous wavefronts," Proc. 2011 IEEE International Conference on Ultra-Wideband, pp. 346–350, 2011.

[4] Y. Wang, Y. Yang, A. E. Fathy, "Experimental assessment of the cross coupling and polarization effects on ultra-wide band see-through-wall imaging reconstruction," IEEE MTT-S International Microwave Symposium Digest, pp. 9–12, June 2009.

[5] A. Nelander, "Switched array concepts for 3-D radar imaging," Proc. 2010 IEEE Radar Conference, pp. 1019–1024, 2010.

[6] T. Counts, A. C. Gurbuz, W. R. Scott Jr., J. H. McClellan, and K. Kim, "Multistatic ground-penetrating radar experiments," IEEE Trans. Geoscience and Remote Sensing, vol. 45, no. 8, pp. 2544–2553, Aug. 2007.

[7] Y. Yang and A. E. Fathy, "Development and implementation of a real-time see-through-wall radar system based on FPGA," IEEE Trans. Geoscience and Remote Sensing, vol. 47, no. 5, pp. 1270–1280, May 2009.

[8] T. Sakamoto, "A fast algorithm for 3-dimensional imaging with UWB pulse radar systems," IEICE Trans. on Communications, vol. E90-B, no. 3, pp. 636–644, 2007.

[9] D. W. Winters, J. D. Shea, E. L. Madsen, G. R. Frank, B. D. Van Veen, S. C. Hagness, "Estimating the Breast Surface Using UWB Microwave Monostatic Backscatter Measurements," IEEE Transactions on Biomedical Engineering, vol. 55, no. 1, pp. 247–256, 2008.

[10] S. Hantscher, A. Reizenzahn, C. G. Diskus, "Through-Wall Imaging With a 3-D UWB SAR Algorithm," IEEE Signal Processing Letters,